

A Block-Sparse Bayesian Learning Algorithm with Dictionary Parameter Estimation for Multi-Sensor Data Fusion

Jakob Möderl*, Anders Malte Westerkamp†, Alexander Venus*, and Erik Leitinger*

*Graz University of Technology, Graz, Austria, {jakob.moederl, a.venus, erik.leitinger}@tugraz.at

†Aalborg University, Aalborg Denmark, amw@es.aau.dk

Abstract—We propose an sparse Bayesian learning (SBL)-based method that leverages group sparsity and multiple parameterized dictionaries to detect the relevant dictionary entries and estimate their continuous parameters by combining data from multiple independent sensors. In a MIMO multi-radar setup, we demonstrate its effectiveness in jointly detecting and localizing multiple objects, while also emphasizing its broader applicability to various signal processing tasks. A key benefit of the proposed SBL-based method is its ability to resolve correlated dictionary entries—such as closely spaced objects—resulting in uncorrelated estimates that improve subsequent estimation stages.

Through numerical simulations, we show that our method outperforms the newtonized orthogonal matching pursuit (NOMP) algorithm when two objects cross paths using a single radar. Furthermore, we illustrate how fusing measurements from multiple independent radars leads to enhanced detection and localization performance.

Index Terms—Sparse Bayesian Learning, Detection, Radar, Sensor Fusion

I. INTRODUCTION

Accurate detection, localization, and tracking of objects is the cornerstone of numerous real-world applications, including ocean science [1], integrated sensing and communications [2], and autonomous robotics [3]. Despite their fundamental importance, these tasks become particularly challenging in scenarios characterized by highly cluttered environments and multiple closely spaced objects. In radar and related applications, the received signal can be modeled as linear combination of the radar’s response to each individual object in the scene. Furthermore, the radar’s response to each object is parameterized by the objects location - the parameter of interest. Jointly estimating (i) then number of components in a superimposed mixture and (ii) the parameters of each component in the mixture is fundamental for detecting and tracking objects, as well as for other related signal processing applications. Jointly addressing (i) and (ii) while fusing multiple observations—such as data from several independent radars monitoring the same area—introduces additional challenges but can also yield significant performance gains, for example, by leveraging the different vantage points of the sensors.

Conventional radar processing chains apply a detect-then-track approach which typically relies on matched filtering in time and space and cell-based detectors, such as the constant false alarm rate (CFAR) detector, for preprocessing the raw

This project was partly funded by the Christian Doppler Laboratory for Location-aware Electronic Systems.

radar signals [4], [5]. The detections of this preprocessing stage are then used as inputs to multiobject tracking (MOT) methods, e.g., based on Bayesian inference [6]–[10]. Such two-step approaches significantly reduce data flow and are computationally efficient. Therefore, they are widely used in practice. Nevertheless, two-step approaches have notable limitations, e.g., when faced with low signal-to-noise ratio (SNR) objects and closely spaced objects whose signals become unresolvable after beamforming. One possible way to address this shortcoming is to use track-before-detect (TBD) methods, which operate directly on matched-filtered radar signals [11]–[15] or even on raw signals [16]–[19], thereby enhancing tracking performance in weak-object scenarios and improving the resolution of closely spaced objects. However, these benefits come at a considerable increase in computational complexity.

We apply an alternate approach to TBD by decreasing the information loss of the preprocessing stage to improve tracking performance. To overcome the limitations of a cell-based detection stage, classic parameter estimation methods such as multiple signal classification (MUSIC) and estimation of signal parameters via rotational invariant techniques (ESPRIT) [20], assume that the number of objects (i.e., the model order) is known, which is typically not the case for radar and similar applications. Sparse signal reconstruction methods, such as the least absolute shrinkage and selection operator (LASSO) [21], matching pursuit (MP) [22] or sparse Bayesian learning (SBL) [23], [24], solve the problem of estimating the number of objects in an efficient way by modeling the observed signal as a product of a large dictionary matrix with a sparse amplitude vector. Thus, the number of objects is indirectly estimated as the number of nonzero amplitudes. Note that many sparse reconstruction methods can be unified within a common framework [25]. In [25], LASSO and MP are classified as Type-I Bayesian methods, whereas SBL belongs to the more general and typically superior Type-II methods. Furthermore, SBL is closely linked to stepwise regression [26] and can be implemented with a computational complexity comparable to that of MP [27].

While initially developed for fixed dictionaries, sparse signal reconstruction methods can be extended to estimate the parameters (e.g., the location of objects) on a continuum by considering a parameterized dictionary matrix [28]–[30], which further helps to improve the performance for correlated (e.g., closely-spaced) objects [31], [32]. Multiple radar-sensors

observing the same scene, i.e., the same objects, result in the amplitude vectors corresponding to each sensor/observation to share the same sparsity-pattern. Thus, resulting in a group-sparse signal reconstruction problem. Naturally, sparse signal reconstruction methods have been extended to group-sparsity, e.g., group-LASSO [33], block-MP [34] or block-SBL [35]–[40]. However, none of these methods estimate the dictionary parameters on a continuum, except for [40] which focuses on group-sparsity within a single observation vector and unknown group-sizes rather than multiple independent observations.

In this work, we propose a novel preprocessing method for sensor fusion between multiple independent sensors (e.g., mutually independent radars) based on SBL to jointly detect relevant dictionary entries and estimate their parameters on the continuum. The proposed SBL-based method extends the block-SBL method introduced in [39] to multiple parameterized dictionary matrices, making it applicable to multi-sensor data fusion. For MOT based on data from multiple radars, our method significantly enhances the measurements used by Bayesian MOT algorithms [6]–[10] by offering (i) more sensitive object-waveform-related detection, (ii) improved resolvability of closely spaced objects, and (iii) reduced measurement correlation for effectively “point-like” detections. The main contributions of this paper are as follows.

- We introduce an SBL-based method that utilizes multiple parameterized dictionaries to detect relevant dictionary entries and estimates the corresponding parameters (on the continuum) by fusing data from multiple independent sensors.
- We apply the proposed algorithm to detect and localize objects in a multiple-input multiple-output (MIMO)-radar setup.
- For a setup consisting of a single MIMO-radar system, we demonstrate that the proposed method outperforms the newtonized orthogonal matching pursuit (NOMP) algorithm [41] when the objects are closely spaced.
- We show that the proposed method is able to fuse the data from multiple independent MIMO-radars to enhance the detection and localization accuracy compared to the single-radar case.

II. SIGNAL MODEL

We consider a multi-radar setup that aims to detect and localize an unknown number of objects with some area of interest by $L \geq 1$ MIMO radars, as illustrated in Figure 1. Each radar consists of N_{Tx} and N_{Rx} co-located receive and transmit antennas, respectively, that surveil the area of interest. Each radar is assumed to processes its own signals fully coherent, i.e., $N_{\text{Tx}} \cdot N_{\text{Rx}}$ channel frequency responses are obtained for each transmission from each radar. The signals from multiple radars are considered to be well separated in time, frequency, or code, so that multiple radars operate independently and do not observe and or interfere with each others signals.

We assume that, after down-conversion to baseband, matched filtering, sampling, and transformation into the fre-

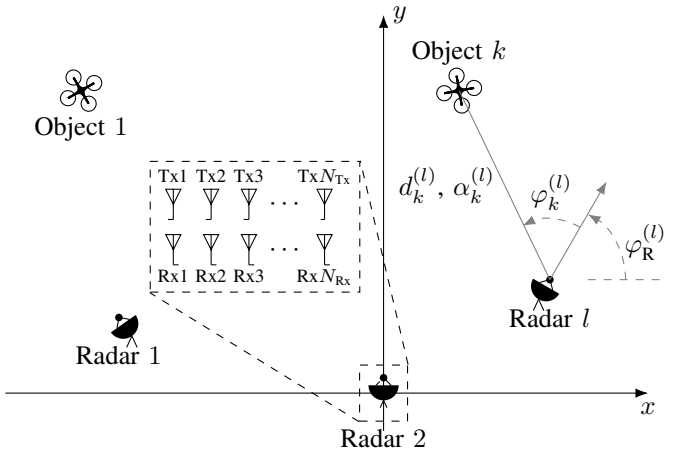


Fig. 1. The scenario considered with an unknown number of objects K , each located at position θ_k being observed by $L \geq 1$ MIMO radars.

quency domain, the received signal at the l th radar ($l = 1, \dots, L$) can be written as

$$\mathbf{y}^{(l)} = \sum_{k=1}^K \psi^{(l)}(\theta_k) \alpha_k^{(l)} + \mathbf{v}^{(l)} \quad (1)$$

where $\mathbf{y}^{(l)} \in \mathbb{C}^{N \times 1}$ is the backscattered signal received by the l th radar from K objects. Here, N_f denotes the number of samples obtained in the frequency domain for each Rx/Tx antenna pair and $N = N_f N_{\text{Tx}} N_{\text{Rx}}$ denotes the total number of available samples per radar. Note that the number of objects K is unknown. The complex amplitude $\alpha_k^{(l)}$ corresponds to the reflection from the k th object, located at $\theta_k = [x_k \ y_k]^T$, in direction of the l th radar. The function $\psi^{(l)}(\theta)$ is the array response of the l th radar to an object at position $\theta = [x \ y]^T$, considering only the direct path. Finally, $\mathbf{v}^{(l)} \in \mathbb{C}^N$ is circularly symmetric complex AWGN with covariance $(\lambda^{(l)} \Lambda_v^{(l)})^{-1}$, where the spectral envelope given by $\Lambda_v^{(l)}$ is assumed to be known (e.g., $\Lambda_v^{(l)} = \mathbf{I}$), but the total noise powers of each sensor, represented by the scalars $\lambda^{(l)}$, $l = 1, \dots, L$, are treated as a nuisance parameters.

In the following, we assume that (i) the signals are narrow-band, (ii) the objects are located in the far-field of the array, and (iii) we consider a MIMO radar with $N_{\text{Tx}} = N_{\text{Rx}} = 3$ transmit and receive antennas. The transmit antennas are spaced with $\lambda_c/2$ each whereas the receive antennas are spaced with λ_c , where λ_c denotes the carrier wavelength, resulting in a virtual linear array with the distances between the elements and the center of the array given by $\mathbf{p} = \lambda_c \cdot [-1.5 \ -1 \ -0.5 \ -0.5 \ 0 \ 0.5 \ 0.5 \ 1 \ 1.5]^T$. The broadside direction of the array is denoted as $\varphi_R^{(l)}$. For each Tx/Rx antenna pair we obtain a channel frequency response sampled at $N_f = 15$ points covering a total bandwidth of 20 MHz. Given assumptions (i)–(iii) above, the response of the l th radar with an array centered at $\theta_R^{(l)} = [x_R^{(l)} \ y_R^{(l)}]^T$ can be factorized into an angle-dependent and a distance-dependent part, i.e., $\psi^{(l)}(\theta) = \frac{1}{\sqrt{N}} (\psi_\varphi(\varphi^{(l)}) \otimes \psi_d(d^{(l)}))$, where $\varphi^{(l)}$ and $d^{(l)}$ are functions of θ , and \otimes denotes the Kronecker-product [42].

Assuming isotropic antennas, the angle-dependent component is given by $\psi_\varphi(\varphi^{(l)}) = e^{-i2\pi \sin(\varphi^{(l)}) p/\lambda_c}$, where e^z (for a vector \mathbf{z}) denotes the element-wise exponential, i is the imaginary unit, and $\varphi^{(l)}$ is the angle of an object located at $\boldsymbol{\theta} = [x \ y]^\top$ relative to $\varphi_R^{(l)}$. The distance-dependent part is $\psi_d(d^{(l)}) = \frac{\lambda_c}{(4\pi)^{3/2}(d^{(l)})^2} e^{-i2\pi(2d^{(l)}/c)f}$, where c is the speed of light and $d^{(l)} = \|\boldsymbol{\theta} - \boldsymbol{\theta}_R^{(l)}\|$ is the distance from the l th radar to $\boldsymbol{\theta}$, with $\|\cdot\|$ denoting the Euclidean norm.¹ The vector $\mathbf{f} = \left[\frac{-N_f+1}{2} \Delta_f \ \frac{-N_f+2}{2} \Delta_f \ \dots \ \frac{N_f-1}{2} \Delta_f \right]^\top$ specifies the equally spaced baseband frequency points at which the signal is sampled, with spacing Δ_f .²

Note that the presented method can be readily generalized—e.g., to other array geometries, wideband models, or completely different sensor modalities—by appropriately choosing $\psi^{(l)}(\boldsymbol{\theta})$ in (1).

III. PROBABILISTIC MODEL AND SPARSE BAYESIAN LEARNING

To estimate the number of objects K , we transform the problem into a sparse signal reconstruction problem such that K is estimated as the number of nonzero components of a sparse vector. Let $K_{\max} \geq K$ be the largest possible number of objects (e.g. $K_{\max} = N$) and $\alpha_k = 0$ for $K < k \leq K_{\max}$ we rewrite (1) as a sparse linear system

$$\mathbf{y}^{(l)} = \Psi^{(l)}(\boldsymbol{\Theta})\boldsymbol{\alpha}^{(l)} + \mathbf{v}^{(l)} \quad (2)$$

where $\boldsymbol{\Theta} = [\boldsymbol{\theta}_1 \ \boldsymbol{\theta}_2 \ \dots \ \boldsymbol{\theta}_{K_{\max}}] \in \mathbb{R}^{2 \times K_{\max}}$ is the joint parameter matrix with each of the K_{\max} columns of $\boldsymbol{\Theta}$ corresponding to the XY-coordinates of a single (potential) object, $\Psi^{(l)}(\boldsymbol{\Theta}) = [\psi^{(l)}(\boldsymbol{\theta}_1) \ \psi^{(l)}(\boldsymbol{\theta}_2) \ \dots \ \psi^{(l)}(\boldsymbol{\theta}_M)]$ is a dictionary matrix consisting of columns $\psi^{(l)}(\boldsymbol{\theta}_k)$, $k = 1, \dots, K_{\max}$, each of which is parameterized by the position $\boldsymbol{\theta}_k$ of a single object, and $\boldsymbol{\alpha}^{(l)} = [\alpha_1 \ \alpha_2 \ \dots \ \alpha_{K_{\max}}]^\top$ is a sparse vector of complex object reflectivities. Specifically, $\boldsymbol{\alpha}^{(l)} = [\alpha_1^{(l)} \ \alpha_2^{(l)} \ \dots \ \alpha_K^{(l)} \ 0 \ \dots \ 0]^\top$, $l = 1, \dots, L$ are vectors with K nonzero elements corresponding to the reflectivities of the K actual objects, and $K_{\max} - K$ zeros. The likelihood of observing $\mathbf{y}^{(l)}$ given $\boldsymbol{\Theta}$ and $\boldsymbol{\alpha}^{(l)}$ is

$$p(\mathbf{y}^{(l)} | \boldsymbol{\alpha}^{(l)}, \boldsymbol{\Theta}, \lambda^{(l)}) = \text{CN}(\mathbf{y}^{(l)}; \Psi^{(l)}(\boldsymbol{\Theta})\boldsymbol{\alpha}^{(l)}, (\lambda^{(l)}\boldsymbol{\Lambda}_v^{(l)})^{-1}) \quad (3)$$

where $\text{CN}(\mathbf{x}; \boldsymbol{\mu}, \boldsymbol{\Sigma}) = |\pi\boldsymbol{\Sigma}|^{-1} e^{-(\mathbf{x}-\boldsymbol{\mu})^\text{H}\boldsymbol{\Sigma}^{-1}(\mathbf{x}-\boldsymbol{\mu})}$ denotes the probability density function (PDF) of multivariate complex Gaussian random variable \mathbf{x} with mean $\boldsymbol{\mu}$ and covariance $\boldsymbol{\Sigma}$, and $(\cdot)^\text{H}$ denotes the hermitian transpose.³ Assuming that the noise $\mathbf{v}^{(l)}$ is independent across all radars $l = 1, \dots, L$ yields the joint likelihood

$$p(\mathbf{Y} | \mathbf{A}, \boldsymbol{\Theta}, \boldsymbol{\lambda}) = \prod_{l=1}^L p(\mathbf{y}^{(l)} | \boldsymbol{\alpha}^{(l)}, \boldsymbol{\Theta}, \lambda^{(l)}) \quad (4)$$

¹With this definition, $|\alpha_k^{(l)}|^2$ corresponds the radar cross section of the k th object in direction of the l th radar, i.e., the unit of $\alpha_k^{(l)}$ is meters.

²The definition of \mathbf{f} given above is used for odd N_f , whereas for even N_f we use $\mathbf{f} = \left[\frac{-N_f}{2} \Delta_f \ \frac{-N_f+1}{2} \Delta_f \ \dots \ \frac{N_f-1}{2} \Delta_f \right]^\top$.

³Note that the proposed method can readily be used for (non-complex) Gaussian models [23].

where $\mathbf{Y} = [\mathbf{y}^{(1)} \ \mathbf{y}^{(2)} \ \dots \ \mathbf{y}^{(L)}]$ is the matrix of all observations $\mathbf{y}^{(l)}$, $\mathbf{A} = [\boldsymbol{\alpha}^{(1)} \ \boldsymbol{\alpha}^{(2)} \ \dots \ \boldsymbol{\alpha}^{(L)}] \in \mathbb{C}^{K_{\max} \times L}$ is the matrix of all amplitudes, consisting of K nonzero rows and $K_{\max} - K$ rows of zeros, and $\boldsymbol{\lambda} = [\lambda^{(1)} \ \lambda^{(2)} \ \dots \ \lambda^{(L)}]^\top$.

A. Sparse Bayesian Learning

To jointly estimate the number of objects K and their positions $\boldsymbol{\theta}_k$, $k = 1, \dots, K$, the proposed multidictionary SBL-based method combines the fast update rule [23], [39], [43], continuous estimation of dictionary parameters [28]–[30], [40], and block-sparse models [37], [39]. To obtain a row-sparse sparse estimate of \mathbf{A} , (i.e., sparse estimates of $\boldsymbol{\alpha}^{(l)}$, $l = 1, \dots, L$, with shared sparsity patterns), we introduce an improper prior with density [24], [39]

$$p(\mathbf{A}) = \prod_{k=1}^{K_{\max}} \sup_{\gamma_k > 0} \left(\prod_{l=1}^L \text{CN}(\alpha_k^{(l)}; 0, \gamma_k^{-1}) \right) \propto \prod_{k=1}^K \frac{1}{(\|\mathbf{A}[k, \cdot]\|^2)^L} \quad (5)$$

that is independent identically distributed across $k = 1, \dots, K_{\max}$, where $\mathbf{A}[k, \cdot]$ denotes the k th row of \mathbf{A} . By omitting the maximization over the hyperparameters $\boldsymbol{\gamma} = [\gamma_1 \ \gamma_2 \ \dots \ \gamma_{K_{\max}}]^\top$ in (5), we obtain a lower bound

$$\tilde{p}(\mathbf{A}; \boldsymbol{\gamma}) = \prod_{l=1}^L \text{CN}(\boldsymbol{\alpha}^{(l)}; 0, \boldsymbol{\Gamma}^{-1}) \leq p(\mathbf{A}) \quad (6)$$

parameterized by $\boldsymbol{\gamma}$, where $\boldsymbol{\Gamma} = \text{diag}(\boldsymbol{\gamma})$ is diagonal matrix with the elements of $\boldsymbol{\gamma}$ along its main diagonal. SBL then proceeds to estimate $\boldsymbol{\Theta}$, $\boldsymbol{\gamma}$ and $\boldsymbol{\lambda}$ by maximizing a lower bound $\mathcal{L}(\boldsymbol{\Theta}, \boldsymbol{\gamma}, \boldsymbol{\lambda})$ on the (log) marginal likelihood $p(\mathbf{Y} | \boldsymbol{\Theta}, \boldsymbol{\lambda})$ of \mathbf{Y} given $\boldsymbol{\Theta}$ and $\boldsymbol{\lambda}$ [24], [25]

$$(\hat{\boldsymbol{\Theta}}, \hat{\boldsymbol{\gamma}}, \hat{\boldsymbol{\lambda}}) = \arg \max_{\boldsymbol{\Theta}, \boldsymbol{\gamma} \succeq 0, \boldsymbol{\lambda}} \mathcal{L}(\boldsymbol{\Theta}, \boldsymbol{\gamma}, \boldsymbol{\lambda}) \quad (7)$$

where

$$\begin{aligned} \mathcal{L}(\boldsymbol{\Theta}, \boldsymbol{\gamma}, \boldsymbol{\lambda}) &= \log \int p(\mathbf{Y} | \mathbf{A}, \boldsymbol{\Theta}, \boldsymbol{\lambda}) \tilde{p}(\mathbf{A}; \boldsymbol{\gamma}) d\mathbf{A} \\ &= \sum_{l=1}^L -(\mathbf{y}^{(l)})^\text{H} (\mathbf{C}^{(l)})^{-1} \mathbf{y}^{(l)} - \log |\mathbf{C}^{(l)}| + \text{const.} \end{aligned} \quad (8)$$

and $\mathbf{C}^{(l)} = \Psi^{(l)}(\boldsymbol{\Theta})\boldsymbol{\Gamma}^{-1}\Psi^{(l)}(\boldsymbol{\Theta})^\text{H} + (\lambda^{(l)}\boldsymbol{\Lambda}_v^{(l)})^{-1}$. That is, the multi-dictionary SBL objective (8) is a sum over classic SBL objective functions [23, Eq. (8)] with each term corresponding to the observations of a single sensor.

Once estimates $\hat{\boldsymbol{\gamma}}$, $\hat{\boldsymbol{\Theta}}$, and $\hat{\boldsymbol{\lambda}}$ are obtained, the (approximate) posterior densities of $\boldsymbol{\alpha}^{(l)}$ conditional on $\mathbf{y}^{(l)}$, $\hat{\boldsymbol{\gamma}}$, $\hat{\boldsymbol{\Theta}}$, and $\hat{\boldsymbol{\lambda}}$ are independent across $l = 1, \dots, L$, i.e., $p(\mathbf{A} | \mathbf{Y}, \hat{\boldsymbol{\Theta}}, \hat{\boldsymbol{\lambda}}; \hat{\boldsymbol{\gamma}}) = \prod_{l=1}^L p(\boldsymbol{\alpha}^{(l)} | \mathbf{y}^{(l)}, \hat{\boldsymbol{\Theta}}, \hat{\boldsymbol{\lambda}}^{(l)}; \hat{\boldsymbol{\gamma}})$, where

$$p(\boldsymbol{\alpha}^{(l)} | \mathbf{y}^{(l)}, \hat{\boldsymbol{\Theta}}, \hat{\boldsymbol{\lambda}}^{(l)}; \hat{\boldsymbol{\gamma}}) = \text{CN}(\boldsymbol{\alpha}^{(l)}; \hat{\boldsymbol{\alpha}}^{(l)}, (\hat{\boldsymbol{\Lambda}}_\alpha^{(l)})^{-1}) \quad (9)$$

with

$$\hat{\boldsymbol{\alpha}}^{(l)} = (\hat{\boldsymbol{\Lambda}}_\alpha^{(l)})^{-1} (\hat{\Psi}^{(l)})^\text{H} \hat{\boldsymbol{\Lambda}}_v^{(l)} \mathbf{y}^{(l)} \quad (10)$$

$$\hat{\boldsymbol{\Lambda}}_\alpha^{(l)} = (\hat{\Psi}^{(l)})^\text{H} \hat{\boldsymbol{\Lambda}}_v^{(l)} \hat{\Psi}^{(l)} + \hat{\boldsymbol{\Gamma}} \quad (11)$$

$\hat{\Lambda}_v^{(l)} = \hat{\lambda}^{(l)} \Lambda_v^{(l)}$, $\hat{\Psi}^{(l)} = \Psi^{(l)}(\hat{\Theta})$, and $\hat{\Gamma} = \text{diag}(\hat{\gamma})$. This approach is known to result in many estimates $\hat{\gamma}_k$ to diverge to infinity and so do the corresponding elements on the main diagonal of $\hat{\Lambda}_\alpha^{(l)}$. Thus, $p(\alpha^{(l)} | \mathbf{y}^{(l)}, \hat{\Theta}, \hat{\lambda}^{(l)}; \hat{\gamma})$ collapses to a Dirac-delta in many dimension resulting in a amplitude vectors $\alpha^{(l)}$ with many elements having value of zero with probability one, i.e., sparse vectors. Furthermore, all $\alpha^{(l)}$ are informed by the same hyperparameters γ and, thus, share the same sparsity pattern.

B. Object Parameter Updates

Finding the global maximum of $\mathcal{L}(\Theta, \gamma, \lambda)$ with respect to all parameters $(\Theta, \gamma, \lambda)$ jointly is computationally prohibitive. Thus, we maximize $\mathcal{L}(\Theta, \gamma, \lambda)$ using coordinate ascent with respect to the tuple of parameters (θ_k, γ_k) corresponding to a single object at a time, while keeping the remaining parameters fixed. Let $\mathbf{M}_{\sim k}^{(l)} = \mathbf{I} - \hat{\Psi}_{\sim k}^{(l)}((\hat{\Psi}_{\sim k}^{(l)})^H \hat{\Lambda}_v^{(l)} \hat{\Psi}_{\sim k}^{(l)} + \hat{\Gamma}_{\sim k})^{-1} (\hat{\Psi}_{\sim k}^{(l)})^H \hat{\Lambda}_v^{(l)}$ and $\hat{\Psi}_{\sim k}^{(l)} = \Psi^{(l)}([\hat{\theta}_1 \hat{\theta}_2 \cdots \hat{\theta}_{k-1} \hat{\theta}_{k+1} \cdots \hat{\theta}_{K_{\max}}])$ denote a matrix of all but the k th column of the dictionary $\hat{\Psi}^{(l)}$, and $\hat{\Gamma}_{\sim k} = \text{diag}(\hat{\gamma}_{\sim k})$ with $\hat{\gamma}_{\sim k}$ as the vector $\hat{\gamma}$ with the k th element removed. Following the derivation of [23], the dependency of $\mathcal{L}(\Theta, \gamma, \lambda)$ on the tuple (θ_k, γ_k) corresponding to the k th object can be made explicit as $\mathcal{L}(\Theta, \gamma, \lambda) = \mathcal{L}_{\sim k} + \ell_k(\theta_k, \gamma_k)$ where $\mathcal{L}_{\sim k}$ is some function that does not depend on (θ_k, γ_k) , and

$$\ell_k(\theta_k, \gamma_k) = \sum_{l=1}^L \frac{|\mu_k^{(l)}(\theta_k)|^2 / s_k^{(l)}(\theta_k)}{1 + \gamma_k s_k^{(l)}(\theta_k)} + \log \frac{\gamma_k s_k^{(l)}(\theta_k)}{1 + \gamma_k s_k^{(l)}(\theta_k)} \quad (12)$$

with

$$s_k^{(l)}(\theta_k) = (\psi^{(l)}(\theta_k)^H \hat{\Lambda}_v^{(l)} \mathbf{M}_{\sim k}^{(l)} \psi^{(l)}(\theta_k))^{-1} \quad (13)$$

$$\mu_k^{(l)}(\theta_k) = s_k^{(l)}(\theta_k) \psi^{(l)}(\theta_k)^H \hat{\Lambda}_v^{(l)} \mathbf{M}_{\sim k}^{(l)} \mathbf{y}^{(l)}. \quad (14)$$

Since there is no analytic solution to the joint maximum of $\ell_k(\theta_k, \gamma_k)$ we resort to coordinate ascent. First, we find

$$\hat{\theta}_k = \arg \max_{\theta} \ell_k(\theta, \hat{\gamma}_k) \quad (15)$$

by means of a numeric optimizer using the previous estimate $\hat{\gamma}_k$. Next, we update $\hat{\gamma}_k$. Taking the derivative of $\ell_k(\hat{\theta}_k, \gamma_k)$ with respect to γ_k yields the fixed point equation

$$0 = \sum_{l=1}^L \frac{1 - \gamma_k (|\mu_k^{(l)}(\hat{\theta}_k)|^2 - s_k^{(l)}(\hat{\theta}_k))}{(1 + \gamma_k s_k^{(l)}(\hat{\theta}_k))^2} \quad (16)$$

which can be solved by finding the solutions to the polynomial equation $P_k(\gamma) = 0$ (i.e., by finding the roots of P_k), where

$$P_k(\gamma) := \sum_{l=1}^L (1 - \gamma (|\mu_k^{(l)}(\hat{\theta}_k)|^2 - s_k^{(l)}(\hat{\theta}_k))) \prod_{j=1, j \neq l}^L (1 + \gamma s_k^{(j)}(\hat{\theta}_k))^2 \quad (17)$$

is a polynomial in γ of degree $2L - 1$. Let $\mathcal{G}_k := \{\gamma > 0 : P_k(\gamma) = 0\}$ denote the set of positive, real-valued roots of P_k , we proceed to update $\hat{\gamma}_k$ using

$$\hat{\gamma}_k = \begin{cases} \arg \max_{\gamma \in \mathcal{G}_k} \ell_k(\hat{\theta}_k, \gamma) & \text{if } \mathcal{G}_k \neq \emptyset \\ \infty & \text{else} \end{cases} \quad (18)$$

where \emptyset denotes the empty set, i.e., we set $\hat{\gamma}_k$ to the solution of (16) that increases $\ell_k(\hat{\theta}_k, \cdot)$ the most.

Single Radar: Lets consider the single-radar case (i.e., $L = 1$) in this paragraph, where we omit the superscript $(\cdot)^{(l)}$ for ease of notation. In this case, (16) has a single positive solution if $|\mu_k(\theta_k)|^2 > s_k(\theta_k)$, whereas no positive solution exists for otherwise [23]. Hence, for any given location θ , $\ell_l(\theta, \cdot)$ achieves its maximum at

$$\gamma_k^*(\theta) = \begin{cases} \frac{1}{|\mu_k(\theta_k)|^2 - s_k(\theta_k)} & \text{if } Q_k(\theta_k) > 1 \\ \infty & \text{else} \end{cases} \quad (19)$$

where $Q_k(\theta) := |\mu_k(\theta)|^2 / s_k(\theta)$ can be recognized as the component SNR [44]. Inserting the optimal value γ_k^* into ℓ_k yields $\ell_k^*(\theta) := \ell_k(\theta, \gamma_k^*(\theta))$, where

$$\ell_k^*(\theta) = \begin{cases} Q_k(\theta) - 1 - \log Q_k(\theta) & \text{if } Q_k(\theta) > 1 \\ 0 & \text{else} \end{cases}. \quad (20)$$

It is straightforward to show, that $\ell_k^*(\theta)$ is an increasing function of the component SNR Q_k . Hence, in the single radar case we find the supremum of $\ell_k(\theta_k, \gamma_k)$ jointly as

$$\hat{\theta}_k = \arg \max_{\theta} Q_k(\theta) \quad (21)$$

$$\hat{\gamma}_k = \gamma_k^*(\hat{\theta}_k) \quad (22)$$

i.e., SBL objective $\mathcal{L}(\Theta, \gamma, \lambda)$ is maximized with respect to the parameters of a single object (θ_k, γ_k) by the position θ that maximizes the component SNR $Q_k(\theta)$ and the object is estimated to have nonzero amplitude if, and only if, the component SNR exceeds unity.

Identical Sensors: Lets assume that the array responses $\psi_k^{(l)} = \psi_k$ and noise distribution (i.e., $\lambda^{(l)} \Lambda_v^{(l)}$) are identical across all $l = 1, \dots, L$, corresponding to, e.g., multiple measurement vectors obtained from the same radar. In this case, the variables $s_k^{(l)} = s_k$ defined in (13) do not depend on l since all $\psi^{(l)}$ are equal such that (16) can be simplified to

$$0 = \frac{1 - \gamma_k (\bar{\mu}_k^2(\hat{\theta}_k) - s_k(\hat{\theta}_k))}{(1 + \gamma_k s_k(\hat{\theta}_k))^2} \quad (23)$$

where $\bar{\mu}_k^2(\hat{\theta}_k) = 1/L \cdot \sum_{l=1}^L |\mu_k^{(l)}(\hat{\theta}_k)|^2$. Hence, the multiple measurement vector case with identical array responses can be treated same as the single measurement vector case $L = 1$, except that $|\mu_k(\hat{\theta}_k)|^2$ is replaced by $\bar{\mu}_k^2(\hat{\theta}_k)$.

Additional Thresholding: It is experimentally known, that the updates for the object parameters (θ_k, γ_k) , $k = 1, \dots, K$ (particular the update of the hyperparameter γ_k governing object existence) described in this section results in a relatively high number of false alarms [44]. To reduce the number of false alarms, we require all detections to exceed a certain component SNR (averaged over $l = 1, \dots, L$). Specifically, when updating the value of $\hat{\gamma}_k$ we use

$$\hat{\gamma}_k = \begin{cases} \arg \max_{\gamma \in \mathcal{G}_k} \ell_k(\hat{\theta}_k, \gamma) & \text{if } \mathcal{G}_k \neq \emptyset \text{ and } \bar{Q}_k(\hat{\theta}_k) > \chi \\ \infty & \text{else} \end{cases} \quad (24)$$

instead of (18), where $\bar{Q}_k(\boldsymbol{\theta}) = 1/L \cdot \sum_{l=1}^L |\mu_k^{(l)}(\boldsymbol{\theta})|^2 / s_k^{(l)}(\boldsymbol{\theta})$ is the component SNR averaged over all radars and $\chi \geq 1$ is the minimum required average component SNR. See [44] for a detailed analysis of the relation between the threshold χ and the false alarm rate for the single radar case.

C. Noise Power Estimate

No closed form solution for the update of the noise parameters $\lambda^{(l)}$ is available. Thus, we resort to an expectation-maximization (EM) update that increases a lower bound $\mathcal{L}^{\text{EM}}(\boldsymbol{\lambda}, \hat{\boldsymbol{\lambda}}^{\text{old}}) \leq \mathcal{L}(\hat{\boldsymbol{\Theta}}, \hat{\boldsymbol{\gamma}}, \boldsymbol{\lambda})$ given the current estimates $\hat{\boldsymbol{\lambda}}^{\text{old}}$, $\hat{\boldsymbol{\Theta}}$ and $\hat{\boldsymbol{\gamma}}$ [45], [46]. We consider \mathbf{Y} as the observed data and (\mathbf{Y}, \mathbf{A}) as the complete data. An improved estimate $\hat{\boldsymbol{\lambda}}^{\text{new}} = \arg \max_{\boldsymbol{\lambda}} \mathcal{L}^{\text{EM}}(\boldsymbol{\lambda}, \hat{\boldsymbol{\lambda}}^{\text{old}})$ is obtained as maximizer of the EM objective

$$\begin{aligned} \mathcal{L}^{\text{EM}}(\boldsymbol{\lambda}, \hat{\boldsymbol{\lambda}}^{\text{old}}) &= \int p(\mathbf{A}|\mathbf{Y}, \hat{\boldsymbol{\Theta}}, \hat{\boldsymbol{\lambda}}^{\text{old}}, \hat{\boldsymbol{\gamma}}) \\ &\quad \times \log p(\mathbf{Y}, \mathbf{A}|\hat{\boldsymbol{\Theta}}, \boldsymbol{\lambda}; \hat{\boldsymbol{\gamma}}) d\mathbf{A} \end{aligned} \quad (25)$$

where $p(\mathbf{Y}, \mathbf{A}|\hat{\boldsymbol{\Theta}}, \boldsymbol{\lambda}; \hat{\boldsymbol{\gamma}}) = p(\mathbf{Y}|\mathbf{A}, \hat{\boldsymbol{\Theta}}, \boldsymbol{\lambda})p(\mathbf{A}; \hat{\boldsymbol{\gamma}})$. Solving the integral and setting the derivative of \mathcal{L}^{EM} to zero yields the estimates

$$\hat{\lambda}^{(l),\text{new}} = \frac{N}{(\hat{\mathbf{y}}_{\text{res}})^H \hat{\boldsymbol{\Lambda}}_v^{(l)} \hat{\mathbf{y}}_{\text{res}} + \text{tr}((\hat{\boldsymbol{\Lambda}}_{\boldsymbol{\alpha}}^{(l)})^{-1} (\hat{\boldsymbol{\Psi}}^{(l)})^H \hat{\boldsymbol{\Lambda}}_v^{(l)} \hat{\boldsymbol{\Psi}}^{(l)})} \quad (26)$$

for $l = 1, \dots, L$, where $\hat{\mathbf{y}}_{\text{res}}^{(l)} = \mathbf{y}^{(l)} - \hat{\boldsymbol{\Psi}}^{(l)} \hat{\boldsymbol{\alpha}}^{(l)}$, $\text{tr}(\cdot)$ is the trace operator, and $\hat{\boldsymbol{\alpha}}^{(l)}$ and $\hat{\boldsymbol{\Lambda}}_{\boldsymbol{\alpha}}^{(l)}$ are the mean and precision, respectively, of $p(\boldsymbol{\alpha}^{(l)}|\mathbf{y}^{(l)}, \hat{\boldsymbol{\Theta}}, \hat{\lambda}^{(l),\text{old}}; \hat{\boldsymbol{\gamma}})$ given by (10) and (11), respectively.

The updates given in subsections III-B and III-C are repeated in a round-robin fashion until convergence or until a fixed number of iterations is exceeded.

IV. ALGORITHM

We define an algorithm by combining the coordinate-ascent updates of estimates $(\hat{\boldsymbol{\theta}}_k, \hat{\gamma}_k)$ together with an initialization and update-schedule as summarized in Algorithm 1.⁴

We start with an empty model $\hat{\gamma}_k = \infty$, $k = 1, \dots, K_{\text{max}}$, and initialize the noise parameters as $\hat{\lambda}^{(l)} = 10 \cdot N / (\mathbf{y}^{(l)})^H \hat{\boldsymbol{\Lambda}}_v^{(l)} \mathbf{y}^{(l)}$. In each iteration, we first go through all “active” objects currently in the model $k \in \{1 \leq k \leq K_{\text{max}} : \hat{\gamma}_k < \infty\}$ and update their estimated positions $\hat{\boldsymbol{\theta}}_k$. To do so, we use a numeric optimizer (Python’s `scipy.optimize`) to maximize

$$\hat{\boldsymbol{\theta}}_k = \arg \max_{\boldsymbol{\theta}} \begin{cases} Q_k(\boldsymbol{\theta}) & \text{if } L = 1 \\ \ell_k(\boldsymbol{\theta}, \hat{\gamma}_k) & \text{if } L > 1 \end{cases} \quad (27)$$

Once $\hat{\boldsymbol{\theta}}_k$ is obtained, we also update $\hat{\gamma}_k$ using (24), potentially setting it to $\hat{\gamma}_k = \infty$ and thereby “deactivating” k th the object. After iterating through all currently existing objects, we search for a new object to detect. To do so, we chose any k corresponding to a “deactivated” object (i.e., $\hat{\gamma}_k = \infty$)

⁴Python code is available at <https://doi.org/10.3217/kcn0n-03509>

Algorithm 1 SBL for Multiple Parameterized Dictionaries

Input: Signals $\mathbf{y}^{(l)}$, $l = 1, \dots, L$, noise precision $\boldsymbol{\Lambda}_v^{(l)}$, array responses $\boldsymbol{\psi}^{(l)} : \mathbb{R}^2 \mapsto \mathbb{C}^{N \times 1}$, threshold χ and grid $\hat{\boldsymbol{\Theta}}$.
Output: Object locations $\hat{\boldsymbol{\Theta}}$, hyperparameters $\hat{\boldsymbol{\gamma}}$, amplitudes $\hat{\boldsymbol{\alpha}}^{(l)}$, $l = 1, \dots, L$, and noise parameter $\hat{\lambda}$.
Initialize $\hat{\lambda}^{(l)} \leftarrow 10 \cdot N / ((\mathbf{y}^{(l)})^H \boldsymbol{\Lambda}_v^{(l)} \mathbf{y}^{(l)})$, and $\hat{\gamma}_k \leftarrow \infty$ for $l = 1, \dots, L$, and $k = 1, \dots, K_{\text{max}}$, respectively.
while not converged **do**
 for $k \in \{1 \leq k \leq K_{\text{max}} : \hat{\gamma}_k < \infty\}$ **do**
 Update $\hat{\boldsymbol{\theta}}_k$ using (27).
 Update $\hat{\gamma}_k$ using (24).
 end for
 $k \leftarrow$ chose any from $\{1 \leq k \leq K_{\text{max}} : \hat{\gamma}_k = \infty\}$.
 $\hat{\boldsymbol{\theta}}_k \leftarrow \arg \max_{\boldsymbol{\theta}} \bar{Q}_k(\boldsymbol{\theta})$.
 Update $\hat{\gamma}_k$ using (24).
 Update $\hat{\lambda}^{(l)}$ for $l = 1, \dots, L$ using (26).
end while
Calculate $\hat{\boldsymbol{\alpha}}^{(l)}$ and $\hat{\boldsymbol{\Lambda}}_{\boldsymbol{\alpha}}^{(l)}$ for $l = 1, \dots, L$ using (10) and (11), respectively.

and find the position of this potential object by finding the position $\hat{\boldsymbol{\theta}}_k$ that maximizes the average component SNR $\bar{Q}_k(\boldsymbol{\theta})$. To aid the numeric optimizer during the search for new objects, we first evaluate $\bar{Q}_k(\boldsymbol{\theta})$ on a sub-Nyquist grid $\hat{\boldsymbol{\Theta}}$ and initialize the numeric optimizer with the location of the maximum on the grid. Again, we use the computed position $\hat{\boldsymbol{\theta}}_k = \arg \max_{\boldsymbol{\theta}} \bar{Q}_k(\boldsymbol{\theta})$ to set $\hat{\gamma}_k$ according to (24), potentially including it as new object in the model. Finally, we update the estimate of the noise parameter $\hat{\lambda}$ using (26). Once the algorithm is converged (or a maximum number of iterations is reached), we also compute the mean and covariance, $\hat{\boldsymbol{\alpha}}^{(l)}$ and $\hat{\boldsymbol{\Lambda}}_{\boldsymbol{\alpha}}^{(l)}$ for $l = 1, \dots, L$, respectively, of the (approximate) posterior $p(\mathbf{A}|\mathbf{Y}, \hat{\boldsymbol{\Theta}}, \hat{\lambda}; \hat{\boldsymbol{\gamma}}) = \prod_{l=1}^L p(\boldsymbol{\alpha}^{(l)}|\mathbf{y}^{(l)}, \hat{\boldsymbol{\Theta}}, \hat{\lambda}^{(l)}; \hat{\boldsymbol{\gamma}})$.

Note that the quantities $\mu_k(\boldsymbol{\theta})$ and $s_k(\boldsymbol{\theta})$ can be computed in an efficient manner by considering the symmetries of the matrix

$$\hat{\boldsymbol{\Lambda}}_v \hat{\mathbf{M}}_{\sim k} = \hat{\boldsymbol{\Lambda}}_v - \hat{\boldsymbol{\Lambda}}_v \hat{\boldsymbol{\Psi}}_{\sim k} (\hat{\boldsymbol{\Psi}}_{\sim k}^H \hat{\boldsymbol{\Lambda}}_v \hat{\boldsymbol{\Psi}}_{\sim k} + \hat{\boldsymbol{\Gamma}}_{\sim k})^{-1} \hat{\boldsymbol{\Psi}}_{\sim k}^H \hat{\boldsymbol{\Lambda}}_v \quad (28)$$

where we omitted the superscript $(\cdot)^{(l)}$ for ease of notation. Let $\mathbf{L}\mathbf{L}^H = \hat{\boldsymbol{\Lambda}}_v$ and $\mathbf{D}\mathbf{D}^H = \hat{\boldsymbol{\Lambda}}_{\boldsymbol{\alpha}}$ be the choleskey decompositions of $\hat{\boldsymbol{\Lambda}}_v$, and $\hat{\boldsymbol{\Lambda}}_{\boldsymbol{\alpha}}$, respectively, and $\mathbf{R} = \hat{\boldsymbol{\Lambda}}_v \hat{\boldsymbol{\Psi}}_{\sim k} \mathbf{D}^{-1}$, such that $\hat{\boldsymbol{\Lambda}}_v \hat{\mathbf{M}}_{\sim k} = \mathbf{L}\mathbf{L}^H - \mathbf{R}\mathbf{R}^H$. Thus we can compute

$$s_k(\boldsymbol{\theta}) = 1 / (\|\mathbf{L}^H \boldsymbol{\psi}(\boldsymbol{\theta})\|^2 - \|\mathbf{R}^H \boldsymbol{\psi}(\boldsymbol{\theta})\|_F^2) \quad (29)$$

$$\mu_k(\boldsymbol{\theta}) = s_k(\boldsymbol{\theta}) \boldsymbol{\psi}(\boldsymbol{\theta})^H \mathbf{y}_{\text{res}} \quad (30)$$

where $\mathbf{y}_{\text{res}} = \hat{\boldsymbol{\Lambda}}_v \mathbf{y} - \mathbf{R}\mathbf{R}^H \mathbf{y}$, and $\|\cdot\|_F$ denotes the Frobenius norm. Here \mathbf{y}_{res} , \mathbf{L} and \mathbf{R} do not depend on $\boldsymbol{\theta}$. Thus, they can be pre-computed for the (numeric) optimization over $\boldsymbol{\theta}$ in (27).

V. RESULTS

A. Single Radar

We assume as single radar ($L = 1$) located at the origin (i.e, $\boldsymbol{\theta}_R^{(1)} = [0 \ 0]^T$) with broadside direction $\varphi_R^{(1)} = \pi/2$ oriented

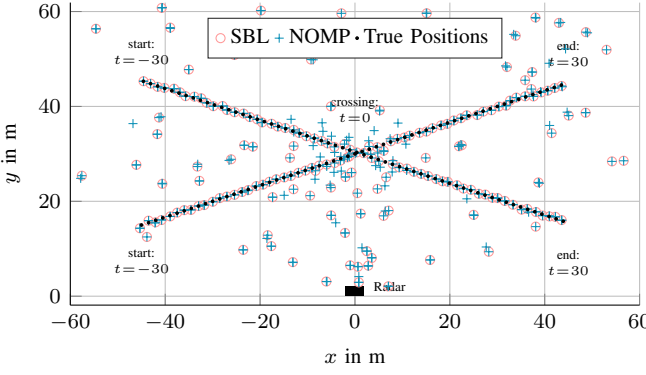


Fig. 2. Tracks crossing at an angle of 36° with component SNR of 20 dB each, and locations of detected objects from SBL and NOMP using low thresholds (7.4 dB for SBL and 7 dB for NOMP). Best viewed in color.

in parallel to the Y-axis. For ease of interpretation, we do not consider a distance-dependent path loss, since the path loss can be absorbed into $\alpha_k^{(l)}$ anyways. Finally, we set $\mathbf{v}^{(1)}$ as additive white Gaussian noise (AWGN) with unit variance, i.e., $\lambda^{(1)} = 1$ and $\Lambda_{\mathbf{v}}^{(1)} = \mathbf{I}$.

We compare the presented SBL algorithm with the NOMP algorithm [41], but instead of using the Newton updates proposed in [41], we employ the same numeric optimizer that is used in our SBL implementation (i.e., Python's `scipy.optimize` function). Note that unlike the proposed SBL algorithm, the NOMP algorithm assumes the noise covariance to be fully known, i.e., it requires all $\lambda^{(l)}$ to be known in addition to $\Lambda_{\mathbf{v}}^{(l)}$. Furthermore, with the parameters given in Section II, the radar has a resolution of roughly 7.5 m in range and 16.5° in angle (corresponding to a cross-range resolution of 8.5 m at a range of 30 m). Thus, the performance of a CFAR detector (or similar grid-based approaches) will be significantly worse than either NOMP or the proposed SBL approach. Similarly, we focus on SBL as method to detect targets in individual time steps, e.g., when used as pre-processing for a multitarget tracking algorithm such as [8]. Thus, we consider a more thorough comparison against tracking algorithms outside the scope of this work.

To evaluate the detection and estimation performance for both, well-separated and closely-spaced objects, we consider two objects that approach one another and cross paths, as depicted in Figure 2. Initially, these objects occupy regions where they are clearly separated in delay. At time step $t = 0$ the objects are located at positions $\theta_1 = [0, 20]^\top$ and $\theta_2 = [0.3, 20.4]^\top$, i.e., separated only by 0.5 m. Note that the distance between the targets corresponds roughly to $|t|$, i.e., at $t \in \{-30, 30\}$ the targets are roughly 30 m apart whereas at $t = 0$ the targets (almost) coincide. As a performance metric, we consider the optimal subpattern assignment (OSPA) [47] with the OSPA order set to two (Euclidean metric) and cutoff distance of 10 m. For each time step we perform 500 Monte-Carlo runs and report the average OSPA. In each realization, the absolute value of the amplitudes $|\alpha_k^{(1)}|$, $k = 1, 2$ is chosen such that the component SNR $\|\psi^{(1)}(\theta_k)\alpha_k^{(1)}\|$ equals 30 dB

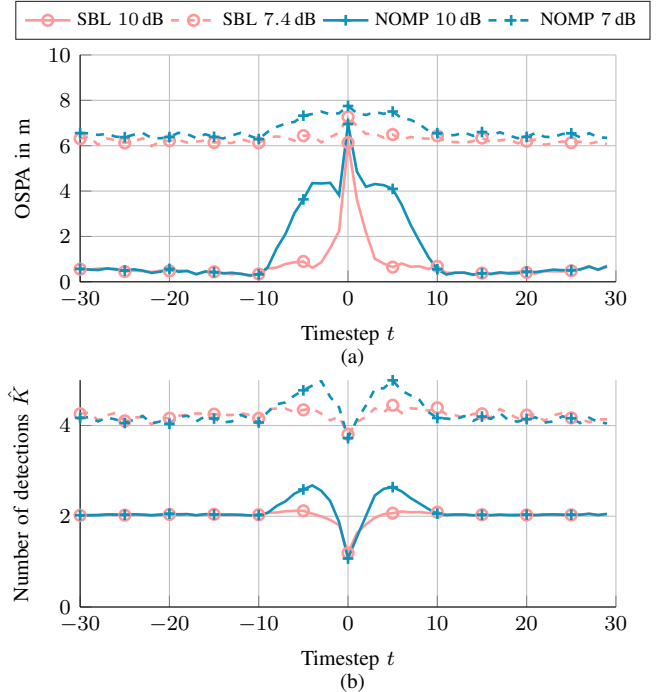


Fig. 3. OSPA (a) and estimated number of objects \hat{K} (b) for crossing tracks with component SNR of 30 dB each. High thresholds (10 dB for both SBL and NOMP) are shown as solid lines and low thresholds (7.4 dB for SBL and 7 dB for NOMP) as dashed lines.

and the phase is drawn uniformly random with limits $[0, 2\pi]$. Both algorithms are evaluated for two different thresholds. To achieve a low false alarm rate of approximately 3.3 %, the thresholds of the algorithms are set to $\chi = 10$ dB for SBL and, equally, a threshold of 10 dB (denoted as τ in [41]) for NOMP. For a higher false alarm rate of approximately two false alarms per time step, we set the thresholds to $\chi = 7.4$ dB for SBL and 7 dB for NOMP.

Figure 3a shows the obtained OSPA whereas Figure 3b shows the estimated model order as function of the time step t . For well separated objects ($|t| > 10$), the performance of both NOMP and SBL is virtually identical in both cases. For medium to small separations ($5 < |t| < 10$), the performance of the SBL algorithm is similar to that of $|t| > 10$, whereas the number of detections (i.e., the false alarm rate) is increased for NOMP, resulting in an increased OSPA as well. For $|t| < 5$, the probability that either of the two algorithms can accurately detect that there are two objects decreases, due the objects close proximity. Thus, the performance of both algorithms deteriorates, with SBL still outperforming NOMP. This is in line with theoretical results concerning the advantages of Type-II Bayesian methods over Type-I Bayesian methods [25].

B. Multiple Radars

To demonstrate the ability of the proposed multi-dictionary SBL algorithm to fuse data from multiple radars, we consider a single object at $\theta_1 = [0, 30]^\top$ with component SNR of 15 dB that is observed by up to four radars located at $\theta_R^{(l)} = [0, 0]^\top$,

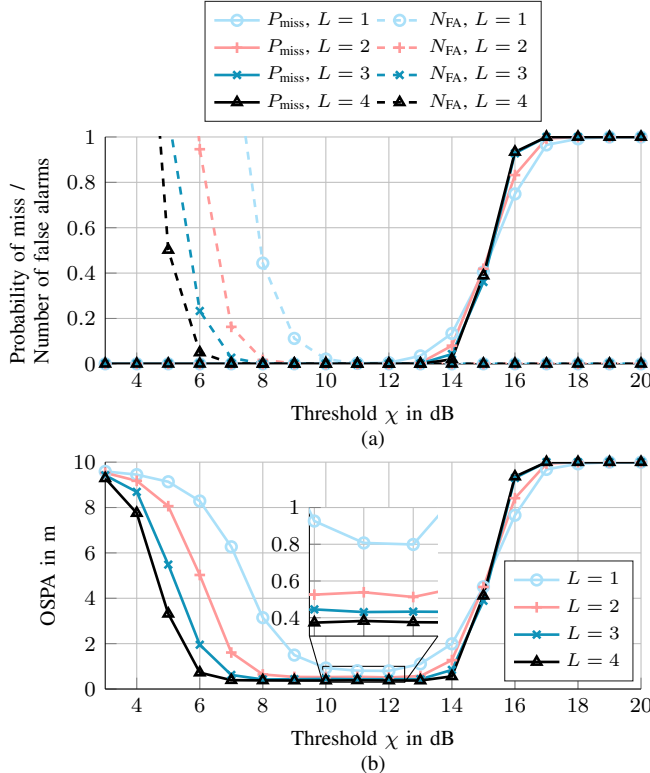


Fig. 4. Detection (a) and localization (b) performance of the proposed SBL algorithm for a single object at $\theta_1 = [0 \ 30]^T$ with a component SNR of 15 dB observed by multiple radars.

$[-30 \ 30]^T$, $[0 \ 60]^T$, and $[30 \ 30]^T$ for $l = 1, \dots, 4$. Each of those radars has a 3×3 MIMO array as described in Section II with broadside direction aimed towards the object and we assume AWGN with unit variance for all radars.

To evaluate the detection performance as function of the threshold χ and the number of radars L , we consider the object to be detected if any estimated object is located within 5 m of the true object location. Depending on the threshold χ , Figure 4a shows the probability of miss detection P_{miss} and the number of false alarms N_{FA} , i.e., the number of estimated objects not located within 5 m of the true object location, averaged over 10^3 Monte-Carlo runs. The number of false alarms reduces with increasing number of radars. This is because, when testing a position θ , the probability that the noise contribution is (jointly) high decreases with the number of (independent) observations. The detection performance is approximately similar for all cases. However, the slope of the missed detection curve is smaller for the single-radar case $L = 1$ compared to $L > 1$. This is again due to the noise interfering either constructively or deconstructively with the signal reflected from the object. This effect is most prominent for $L = 1$ and reduces for increasing L due to the noise-averaging effect of multiple observations. In short, increasing the number of radars helps to decrease the number of false alarms. Equivalently, this allows the use of a smaller detection threshold to increase the detection performance in low-SNR

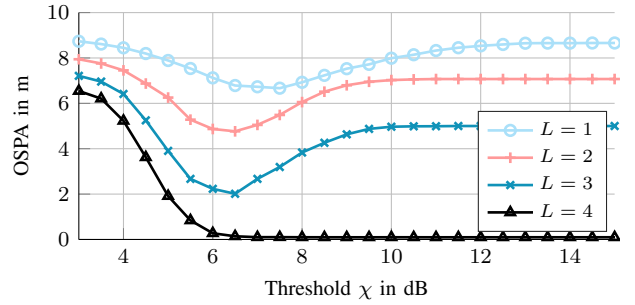


Fig. 5. OSPA of the proposed SBL algorithm for four objects observed by up to four radars when considering the path loss.

cases.

The localization performance (in terms of the OSPA) is shown in Figure 4b. For high thresholds ($\chi \geq 15$ dB), the OSPA is dominated by missed detections. For small thresholds (depending on the number of radars L , e.g., $\chi < 8$ dB for $L = 1$), the OSPA is dominated by false alarms. In between, e.g., for a threshold of $\chi = 11$ dB, there are almost no miss detections or false alarms (see Figure 4a). Therefore the OSPA reflects the localization accuracy. It can be seen, that for $\chi = 11$ dB an OSPA of 0.84 m, 0.53 m, 0.43 m, and 0.37 m is achieved for $L = 1, 2, 3, 4$, respectively.

As a second multi-radar example, we simulate four objects at positions $\theta_k = [0 \ 10]^T$, $[20 \ -30]^T$, $[0 \ 50]^T$, and $[20 \ 30]^T$ for $k = 1, \dots, 4$. All four objects are observed by up to four radars with the same positions as before. In this case, we consider the distance-dependent path loss and set the objects amplitudes $\alpha_k^{(l)}$ such that a component SNR of 30 dB is achieved at a distance of 10 m. Figure 5 shows the OSPA achieved by the proposed algorithm for varying thresholds χ . In this case, each additional radar improves the OSPA by a wide margin, due to the different radars achieving high SNRs in different regions of the surveilled area.

VI. CONCLUSION

We introduced a multidictionary SBL algorithm that jointly detects and estimates dictionary parameters on a continuum across multiple sensors. The algorithm has been used to detect and localize objects by fusing data from multiple MIMO radars. In the single-radar setting, the proposed multidictionary SBL algorithm outperforms the NOMP algorithm [41], especially when multiple objects are closely spaced. We illustrate how combining data from multiple radars can reduce the false alarm rate and improve localization accuracy. By choosing an appropriate parameterized dictionary, the same multidictionary algorithm can be adapted to other applications, e.g., direction of arrival estimation in multi-frequency ocean acoustic channels [38].

REFERENCES

- [1] J. Jang, F. Meyer, E. R. Snyder, S. M. Wiggins, S. Baumann-Pickering, and J. A. Hildebrand, "Bayesian detection and tracking of odontocetes in 3-D from their echolocation clicks," *J. Acoust. Soc.*, vol. 153, no. 5, pp. 2690–2705, May 2023.

[2] N. González-Prelicic, M. Furkan Keskin, O. Kaltiokallio, M. Valkama, D. Dardari, X. Shen, Y. Shen, M. Bayraktar, and H. Wymeersch, "The integrated sensing and communication revolution for 6g: Vision, techniques, and applications," *Proc. IEEE*, vol. 112, no. 7, pp. 676–723, July 2024.

[3] J. Levinson, J. Askeland, J. Becker, J. Dolson, D. Held, S. Kammel, J. Z. Kolter, D. Langer, O. Pink, V. Pratt, M. Sokolsky, G. Stanek, D. Stavens, A. Teichman, M. Werling, and S. Thrun, "Towards fully autonomous driving: Systems and algorithms," in *IEEE Intell. Vehicles Symp.*, Baden-Baden, Germany, Jun. 5–9, 2011, pp. 163–168.

[4] R. Nitzberg, "Constant-false-alarm-rate signal processors for several types of interference," *IEEE Trans. Aerosp. Electron. Syst.*, vol. AES-8, no. 1, pp. 27–34, Feb. 1972.

[5] S. Mallat and Z. Zhang, "Matching pursuits with time-frequency dictionaries," *IEEE Trans. Signal Process.*, vol. 41, no. 12, pp. 3397–3415, Dec. 1993.

[6] Y. Bar-Shalom, P. K. Willett, and X. Tian, *Tracking and Data Fusion: A Handbook of Algorithms*. Storrs, CT, USA: Yaakov Bar-Shalom, 2011.

[7] R. Mahler, *Statistical Multisource-Multitarget Information Fusion*. Norwood, MA, USA: Artech House, Inc., 2007.

[8] F. Meyer, T. Kropfreiter, J. L. Williams, R. Lau, F. Hlawatsch, P. Braca, and M. Z. Win, "Message passing algorithms for scalable multitarget tracking," *Proc. IEEE*, vol. 106, no. 2, pp. 221–259, Feb. 2018.

[9] X. Li, E. Leitinger, A. Venus, and F. Tufvesson, "Sequential detection and estimation of multipath channel parameters using belief propagation," *IEEE Trans. Wireless Commun.*, vol. 21, no. 10, pp. 8385–8402, Apr. 2022.

[10] A. Venus, E. Leitinger, S. Tertinek, F. Meyer, and K. Witrisal, "Graph-based simultaneous localization and bias tracking," *IEEE Trans. Wireless Commun.*, vol. 23, no. 10, pp. 13 141–13 158, May 2024.

[11] S. J. Davey, M. Wieneke, and H. Vu, "Histogram-PMHT unfettered," *IEEE J. Sel. Topics Signal Process.*, vol. 7, no. 3, pp. 435–447, Mar. 2013.

[12] F. Papi, B.-N. Vo, B.-T. Vo, C. Fantacci, and M. Beard, "Generalized labeled multi-Bernoulli approximation of multi-object densities," *IEEE Trans. Aerosp. Electron. Syst.*, vol. 63, no. 20, pp. 5487–5497, July 2015.

[13] B. Ristic, L. Rosenberg, D. Y. Kim, X. Wang, and J. Williams, "Bernoulli track-before-detect filter for maritime radar," *IET Radar, Sonar & Navigation*, vol. 14, no. 3, pp. 356–363, Feb. 2020.

[14] T. Kropfreiter, J. L. Williams, and F. Meyer, "A scalable track-before-detect method with Poisson/multi-Bernoulli model," in *2021 IEEE 24th Int. Conf. Inf. Fusion*, Sun City, South Africa, Nov. 1–4, 2021, pp. 1–8.

[15] —, "Multiobject tracking for thresholded cell measurements," in *27th Int. Conf. Inf. Fusion*. IEEE, Jul. 8–11, 2024, pp. 1–8.

[16] A. M. Westerkam, J. Möderl, E. Leitinger, and T. Pedersen, "Variational message passing-based multiobject tracking for MIMO-radar using raw sensor signals," in *28th IEEE Int. Conf. Inf. Fusion*, Rio de Janeiro, Brazil, Mar. 7–11, 2025.

[17] M. Liang, E. Leitinger, and F. Meyer, "A belief propagation approach for direct multipath-based SLAM," in *Proc. Asilomar-23*, Pacific Grove, CA, USA, Nov. 2023.

[18] —, "Direct multipath-based SLAM," *IEEE Trans. Signal Process.*, 2025.

[19] M. Liang and F. Meyer, "An approach of directly tracking multiple objects," in *Proc. Asilomar-24*, Pacific Grove, CA, USA, 2024.

[20] P. Stoica and R. Moses, *Spectral analysis of signals*. Upper Saddle River, NJ, USA: Pearson Prentice Hall, 2005.

[21] R. Tibshirani, "Regression shrinkage and selection via the LASSO," *J. Roy. Statistical Soc.: Ser. B (Statistical Methodology)*, vol. 58, no. 1, pp. 267–288, 1996.

[22] S. Mallat and Z. Zhang, "Matching pursuits with time-frequency dictionaries," *IEEE Trans. Signal Process.*, vol. 41, no. 12, pp. 3397–3415, 1993.

[23] A. Faul and M. Tipping, "Analysis of sparse Bayesian learning," in *Advances Neural Inf. Process. Syst.*, vol. 14, Vancouver, Canada, Dec. 3–8, 2001, pp. 383–389.

[24] J. Palmer, B. Rao, and D. Wipf, "Perspectives on sparse Bayesian learning," in *Adv. Neural Inf. Process. Syst.*, vol. 16, Vancouver, Canada, Dec. 8–13, 2003, pp. 249–256.

[25] D. P. Wipf, B. D. Rao, and S. Nagarajan, "Latent variable Bayesian models for promoting sparsity," *IEEE Trans. Inf. Theory*, vol. 57, no. 9, pp. 6236–6255, Sep. 2011.

[26] S. E. Ament and C. P. Gomes, "Sparse Bayesian learning via stepwise regression," in *Proc. 38th Int. Conf. Mach. Learn.*, Jul. 18–24, 2021.

[27] R. R. Pote and B. D. Rao, "Light-weight sequential SBL algorithm: An alternative to OMP," in *IEEE Int. Conf. Acoustics, Speech and Signal Process.*, Rhodes Island, Greece, Jun. 04–10, 2023.

[28] T. L. Hansen, M. A. Badiu, B. H. Fleury, and B. D. Rao, "A sparse Bayesian learning algorithm with dictionary parameter estimation," in *IEEE 8th Sensor Array and Multichannel Signal Process. Workshop*, A Coruna, Spain, Jun. 22–25, 2014, pp. 385–388.

[29] S. Grebien, E. Leitinger, K. Witrisal, and B. H. Fleury, "Super-resolution estimation of UWB channels including the dense component – An SBL-inspired approach," *IEEE Trans. Wireless Commun.*, vol. 23, no. 8, pp. 10 301–10 318, Feb. 2024.

[30] T. L. Hansen, B. H. Fleury, and B. D. Rao, "Superfast line spectral estimation," *IEEE Trans. Signal Process.*, vol. 66, no. 10, pp. 2511–2526, Feb. 2018.

[31] M. F. Duarte and R. G. Baraniuk, "Spectral compressive sensing," *Appl. Comput. Harmon. Anal.*, vol. 35, no. 1, pp. 111–129, Jul. 2013.

[32] Y. Chi, L. L. Scharf, A. Pezeshki, and A. R. Calderbank, "Sensitivity to basis mismatch in compressed sensing," *IEEE Trans. Signal Process.*, vol. 59, no. 5, pp. 2182–2195, May 2011.

[33] M. Yuan and Y. Lin, "Model selection and estimation in regression with grouped variables," *J. Roy. Statistical Soc.: Ser. B (Statistical Methodology)*, vol. 68, no. 1, pp. 49–67, Feb. 2006.

[34] Y. C. Eldar, P. Kupinger, and H. Bolcskei, "Block-sparse signals: Uncertainty relations and efficient recovery," *IEEE Trans. Signal Process.*, vol. 58, no. 6, pp. 3042–3054, Jun. 2010.

[35] Z. Zhang and B. D. Rao, "Extension of SBL algorithms for the recovery of block sparse signals with intra-block correlation," *IEEE Trans. Signal Process.*, vol. 61, no. 8, pp. 2009–2015, Apr. 2013.

[36] M. Luessi, S. D. Babacan, R. Molina, and A. K. Katsaggelos, "Bayesian simultaneous sparse approximation with smooth signals," *IEEE Trans. Signal Process.*, vol. 61, no. 22, pp. 5716–5729, Nov. 2013.

[37] S. D. Babacan, S. Nakajima, and M. N. Do, "Bayesian group-sparse modeling and variational inference," *IEEE Trans. Signal Process.*, vol. 62, no. 11, pp. 2906–2921, Jun. 2014.

[38] S. Nannuru, K. L. Gemba, P. Gerstoft, W. S. Hodgkiss, and C. F. Mecklenbräuker, "Sparse Bayesian learning with multiple dictionaries," *Signal Processing*, vol. 159, pp. 159–170, June 2019.

[39] J. Möderl, E. Leitinger, B. H. Fleury, F. Pernkopf, and K. Witrisal, "Fast variational block-sparse Bayesian learning," *IEEE Trans. Signal Process.*, 2025.

[40] J. Möderl, F. Pernkopf, K. Witrisal, and E. Leitinger, "Variational inference of structured line spectra exploiting group-sparsity," *IEEE Trans. Signal Process.*, Nov. 2024.

[41] B. Mamandipoor, D. Ramasamy, and U. Madhow, "Newtonized orthogonal matching pursuit: Frequency estimation over the continuum," *IEEE Trans. Signal Process.*, vol. 64, no. 19, pp. 5066–5081, Oct. 2016.

[42] A. Richter, "Estimation of radio channel parameters: Models and algorithms," PhD Thesis, Ilmenau University of Technology, Mar. 2005.

[43] D. Shutin, T. Buchgraber, S. R. Kulkarni, and H. V. Poor, "Fast variational sparse Bayesian learning with automatic relevance determination for superimposed signals," *IEEE Trans. Signal Process.*, vol. 59, no. 12, pp. 6257–6261, Dec. 2011.

[44] E. Leitinger, S. Grebien, B. Fleury, and K. Witrisal, "Detection and estimation of a spectral line in MIMO systems," in *2020 54th Asilomar Conf. Signals, Syst. and Computers*, Pacific Grove, CA, USA, Nov. 01–04, 2020, pp. 1090–1095.

[45] C. M. Bishop, *Pattern Recognition and Machine Learning*. Secaucus, NJ, USA: Springer-Verlag New York, Inc., 2006.

[46] D. G. Tzikas, A. C. Likas, and N. P. Galatsanos, "The variational approximation for Bayesian inference," *IEEE Signal Process. Mag.*, vol. 25, no. 6, pp. 131–146, Nov. 2008.

[47] D. Schuhmacher, B.-T. Vo, and B.-N. Vo, "A consistent metric for performance evaluation of multi-object filters," *IEEE Trans. Signal Process.*, vol. 56, no. 8, pp. 3447–3457, Aug. 2008.